

# Changes in the saltation flux following a step-change in macro-roughness

John A. Gillies,<sup>1\*</sup>  Vicken Etyemezian,<sup>1</sup> George Nikolich,<sup>1</sup> William G. Nickling<sup>2</sup> and Jasper F. Kok<sup>3</sup>

<sup>1</sup> Division of Atmospheric Sciences, Desert Research Institute, Reno, NV USA

<sup>2</sup> Department of Geography, University of Guelph, Guelph, ON Canada

<sup>3</sup> Atmospheric and Oceanic Sciences, University of California, Los Angeles, CA USA

Received 7 September 2017; Revised 5 January 2018; Accepted 5 February 2018

\*Correspondence to: John A. Gillies, Division of Atmospheric Sciences, Desert Research Institute, Reno, NV, USA. E-mail: jackg@dri.edu

# ESPL

Earth Surface Processes and Landforms

**ABSTRACT:** The effect of a step change in macro-roughness on the saltation process under sediment supply limited conditions was examined in the atmospheric boundary layer. For an array of roughness elements of roughness density  $\lambda = 0.045$  ( $\lambda$  = total element frontal area/total surface area of the array) the horizontal saltation flux was reduced by 90% ( $\pm 7\%$ ) at a distance of  $\approx 150$  roughness element heights into the array. This matches the value predicted using an empirical design model and provides confidence that it can be effectively used to engineer roughness arrays to meet sand flux reduction targets. Measurements of the saltation flux characteristics in the vertical dimension, including: saltation layer decay (e-folding) height and particle size, revealed that with increasing distance into the array, the rate of mass flux change with increasing height decreased notably, and (geometric) mean particle diameter decreased. The distribution of the saltation mass flux in the vertical remains exponential in form with increasing distance into the roughness array, and the e-folding height increases as well as increasing at a greater rate as particle diameter diminishes. The increase in e-folding height suggests the height of saltating particles is increasing along with their mean speed. This apparent increase in mean speed is likely due to the preferential removal, or sequestration, of the slower moving particles across the size spectrum, as they travel through the roughness array. Copyright © 2018 John Wiley & Sons, Ltd.

**KEYWORDS:** saltation flux; macro-roughness; e-folding height; mean particle size changes

## Introduction

Wind blowing over a surface with loose sand that exceeds a critical shear stress on the surface will entrain these particles and move them downwind as bedload in three recognized modes of transport: creep, reptation, and saltation. The characterization of the saltation flux, in which particles move in a series of repeated ejections and travel in ballistic trajectories followed by impact on the surface has garnered considerable research effort in the earth sciences. The saltation process plays critical roles in aeolian bedform development across multiple scales (e.g. Anderson, 1987; Claudin and Andreotti, 2006; Dúran *et al.*, 2011; Gillies *et al.*, 2012; Parteli *et al.*, 2014; Schmerler *et al.*, 2016) and is a dominant mechanism driving the emission of dust-sized particles, which represent the suspended load in aeolian transport (e.g. Shao *et al.*, 1993; Shao, 2001; Kok *et al.*, 2012).

It is now generally acknowledged that the horizontal mass flux of wind-driven sand decreases exponentially with elevation above the surface (e.g. Bagnold, 1941; Chepil, 1945; Williams, 1964; Sørensen, 1985; Namikas, 2003; Farrell and Sherman, 2006, 2013; Martin and Kok, 2017a) and the general form of the relationship is:

$$Q(z) = Q_0 \exp(-z/z_q) \quad (1)$$

where  $Q(z)$  is the streamwise mass flux at elevation  $z$  above the bed,  $Q_0$  is the scaling parameter for the profile and  $z_q$  the characteristic saltation layer decay height (i.e. the e-folding height). The magnitude of  $z_q$  depends on the typical hop height  $z_{\text{hop}}$  of saltating particles (Bagnold, 1941; Owen, 1964; Ungar and Haff, 1987; Namikas, 2003). That is (Martin and Kok, 2017a),

$$z_q = C_Q z_{\text{hop}} \quad (2)$$

where  $C_Q$  is a dimensionless constant of order one. For ballistic trajectories, the hop height  $z_{\text{hop}}$  depends on the vertical speed,  $v_{zo}$  (in  $\text{m s}^{-1}$ ) with which saltating particles leave the surface upon rebound or ejection:

$$z_{\text{hop}} = \frac{v_{zo}^2}{2g} \quad (3)$$

where  $g$  is the acceleration due to gravity (in  $\text{m s}^{-2}$ ). Since  $v_{zo}$  is closely linked to the mean particle speed (Owen, 1964; Kok, 2010), Equations (1)–(3) imply that the e-folding height  $z_q$  is a sensitive function of the mean particle speed. In other words, a measured increase (decrease) in  $z_q$  denotes an increase (decrease) in mean particle speed.

Observations of the change in mean grain size as a function of height show complex patterns including a decrease in mean grain size with height (Williams, 1964; Li *et al.*, 2008) while

other available data reveal instances of an increase in mean grain size with height (Williams, 1964; Xing, 2007; Speirs *et al.*, 2008; Gillies *et al.*, 2013). Additionally, it has often been observed that at some distance above the surface the grain size trend can reverse (Williams, 1964; Xing, 2007; Farrell *et al.*, 2012; Zhang *et al.*, 2017), which may be indicative of a change in transport system dynamics (Andreotti, 2004). The available data on particle size relationships in the vertical and horizontal dimensions do not present a simple or consistent picture of grain motions and trajectories leading to a unified model for a bed of mixed particle sizes.

Recent research has documented the change in the mass flux of particles in saltation as the saltation cloud moves from relatively flat, unobstructed flow conditions to one in which the flow encounters and is perturbed by the presence of large roughness elements (e.g. Gillies *et al.*, 2006, 2007, 2014, 2015; Gillies and Lancaster, 2013). Measurements of the saltation flux exterior and interior to a change of roughness show clearly that the mass flux decreases exponentially with increasing distance into the roughness, reaching a new equilibrium flux at >100 roughness element heights (Gillies *et al.*, 2015). The rate of change of the mass flux with distance and the resultant roughness adjusted saltation flux scale with the roughness density ( $\lambda$ ) (Gillies *et al.*, 2015):

$$\lambda = n b h / S \quad (4)$$

where  $n$  is the number of roughness elements occupying the area  $S$  (in  $\text{m}^2$ ),  $b$  is element breadth (in meters), and  $h$  is element height (in meters). Both Gillies and Lancaster (2013) and Gillies *et al.* (2015) report this scaling relationship based on spatially-distributed measurements of saltation mass flux at only one height above the surface, which allowed for a comparison of the spatial characteristics of the mass flux in response to its interaction with large roughness elements.

Although this recent research has established that the change in saltation mass flux at a specific height scales as a function of  $\lambda$  as it responds to the presence of macro-roughness, it has not examined how the scaling changes over the vertical dimension. It has also not been determined if the observed change in mass flux is accompanied by a change in the mean grain diameter.

Understanding how large roughness elements affect sand transport is important as there are many natural surfaces where sand transport occurs among large roughness elements including vegetation or sediment mounds covered in vegetation, for example nebkhas (Wolfe and Nickling, 1994; Al-Awadhi, 2014; Gillies *et al.*, 2014), or varying amounts of solid roughness elements composed of rocks (Gillies *et al.*, 2010, 2013; Lancaster *et al.*, 2010). Arrays of large roughness elements that have been manufactured have been tested to evaluate their effectiveness to serve as a method to reduce sand transport and the associated dust emissions, for example, at the Keeler Dunes, Keeler, CA (Gillies *et al.*, 2015). Increased understanding of how roughness modulates saltation, which in turn affects the dust emission process, may result in improved saltation and dust flux models that account for roughness effects and also ways to better use roughness to reduce dust emissions, improve air quality, and meet air quality standards.

In this work, we present results from a field study where changes in vertical profiles of sand flux and particle size, before and after encountering regularly spaced roughness elements, were measured to quantify the effect of the step change in roughness. By carrying out this study in a field setting there were no constraints on the saltation system, the boundary layer flow, or the size of the roughness elements that were used, as would be the case for wind tunnel-based experiments (White and Mounla, 1991; Sherman and Farrell, 2008). The supply of sediment,

however, was not unlimited upwind of the array of roughness, nor were the elements resting on a deformable bed of sand.

## Materials and Methods

A new set of time-integrated, particle size distribution- and height-resolved mass saltation flux profiles were collected as saltating particles traveled through an array of macro-roughness elements in the atmospheric inertial sublayer in 2015 and 2016. This was carried out as part of an experiment to evaluate methods to reduce sand transport and dust emissions at Owens Lake, CA, which is a source of dust known to contribute to local and regional air quality degradation (Ono *et al.*, 2011). Measurement of the vertical saltation flux profiles were made upwind of, and at defined distances through, a large array of large roughness elements to investigate how the mass flux is affected in the vertical and along-wind directions by a step-change in roughness.

### The roughness elements and the roughness array

The roughness elements used in this experiment were commercially manufactured, rectangular plastic bins (model SNT300) with the dimensions of an individual element being: 0.725 m (length)  $\times$  0.38 m (height)  $\times$  0.45 m (width). The roughness elements were placed and organized into a staggered array pattern of fixed dimensions on an area of crusted playa surface at Owens Lake, CA, where sand transport was also known to occur (Figure 1). The open fetch upwind of the northerly and southerly edges of the array well-exceeded 500 m. The roughness array was composed of 1620 elements with the length dimension of the elements set perpendicular to the predominantly bi-modal wind directions of 147° and 327°, determined from a 21 year record from a nearby 10 m high meteorological tower operated by the Great Basin Unified Air Pollution Control District (Bishop, CA). The center-to-center spacing between elements was 2.48 m as was the row-to-row distance (Figures 1 and 2). The elements were weighted down by adding sediment to prevent them from being shifted by strong winds. The length and width of the array was 100 m, creating an area of 1 ha with  $\lambda = 0.045$ . The normalized (total) sand flux ( $\text{NSF}_T$ , the ratio of sand flux measured internal to the array to that measured upwind and external to the array) was expected to be 0.10 for sediment in transport deep into the roughness array (i.e. horizontal distance >100 element heights) based on Gillies *et al.*'s (2015) equation (Equation (4)).

### Sand flux and wind instrumentation

The test area was instrumented to measure sand flux external and internal to the array. Table I defines the positions of the instruments relative to the roughness array. Sand flux was measured using modified BSNE-style traps (Fryrear, 1986) as described by Gillies *et al.* (2012, 2013), which they used to measure sand flux in the McMurdo Dry Valleys in Antarctica. The version used here did not make use of the automated opening and closing of the trap inlets. Briefly, the traps have four wedge-shaped compartments that self-orient into the wind (Figure 3). Each trap had four catchers spaced logarithmically with heights between  $\approx 0.17$  m and  $\approx 1.3$  m. The opening of each catcher is 0.02 m  $\times$  0.05 m. The total collection volume per receptacle is approximately 0.0025  $\text{m}^3$ . The four catchers are connected through the tail fin assembly, which keeps them all facing the same direction and aligned into the wind. By



**Figure 1.** The roughness array on Owens Lake, CA. The view into the frame is towards the south and the dimensions of the roughness array are  $\approx 100 \text{ m} \times \approx 100 \text{ m}$  (Photo credit: J. Juchtzer). [Colour figure can be viewed at [wileyonlinelibrary.com](http://wileyonlinelibrary.com)]

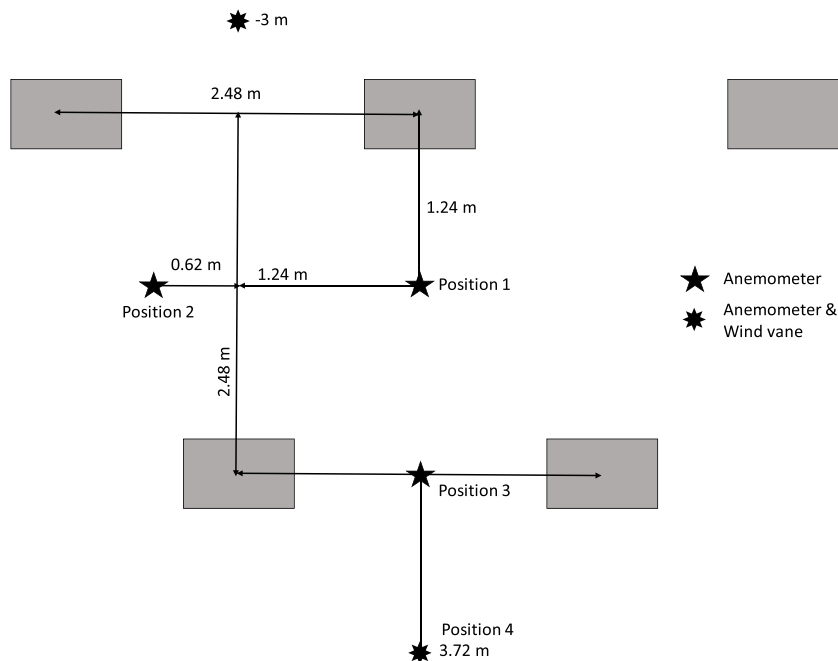


**Figure 2.** The spacing of the elements and the positions of the near surface anemometers and wind vane with respect to the roughness elements (gray rectangles). The pattern of near surface anemometers and wind vanes is repeated at four locations through to 50 m into the roughness array. [Colour figure can be viewed at [wileyonlinelibrary.com](http://wileyonlinelibrary.com)]

convention, the lowest trap compartment is one, the highest four. Eight traps were used in this experiment. By convention, the trap furthest to the north is designated as one, the furthest south as eight. The traps interior to the array were set  $\approx 2.5 \text{ m}$  from the centerline with the offset staggered to the west and then the east for successive traps through the array. In addition, 30 Cox Sand Catchers, a single measurement height trap (Gillies *et al.*, 2015), were placed into the roughness array with their annular opening at 15 cm above the surface. Eight were collocated with the BSNE traps and the remaining were located at the same positions as the BSNE traps, with one along the centerline, and the other two half way to the edge on either side of the centerline. This allowed for a more spatially diverse measurement of saltation flux through the roughness array.

Wind speed at five heights above ground level (1.25 m, 2.20 m, 3.87 m, 6.82 m, and 10 m) and wind direction at 10 m were measured on four 10 m towers. Their positions exterior and interior to the array are provide in Table I. To characterize the airflow among the roughness elements 20 anemometers and four wind vanes were placed external and internal to the array at a height of 0.25 m above ground level (AGL). This is 0.13 m below the top of the roughness elements. One anemometer and one wind vane were placed 3 m upwind of the centerline of the array also at 0.25 m AGL on the north end of the array. The other 19 anemometers and four wind vanes were placed inside the array from its northern boundary extending  $\approx 50 \text{ m}$  into the array. The positions of the anemometers and wind vanes relative to the roughness elements are shown in Figure 2 and this



**Table 1.** The positions of the instruments relative to the roughness array

Instrument	Between rows (from north edge)	Horizontal distance (from north edge) (m)	Normalized distance <sup>a</sup> (ND, from upwind [north] edge defined as zero to southern edge defined as 260.0)
Trap 1	N/A (exterior)	-10.0	0
Trap 2	3–4	6.2	16.3
Trap 3	8–9	18.6	48.9
Trap 4	16–17	38.5	101.2
Trap 5	26–27	60.8	159.9
Trap 6	33–34	80.6	212.1
Trap 7	38–39	93.0	244.7
Trap 8	N/A (exterior)	110.0	261.0
Tower 1	N/A (exterior)	-10.0	0
Tower 2	16–17	38.4	101.2
Tower 3	25–26	60.8	159.9
Tower 4	N/A (exterior)	110.0	261.0

<sup>a</sup>ND = horizontal distance/element height.

Note: N/A, not available.

pattern is repeated four times between the northern edge of the roughness array and halfway through ( $\approx 50$  m).

### Particle size distribution measurements

Sediment samples retrieved from the trap compartments were returned to the laboratory for gravimetric and particle size analysis. The sediment samples were weighed on an electronic balance (Model MS1602S, Mettler-Toledo, Columbus, OH) to a precision of 0.01 g. Following the weighing, sediment samples were submitted for particle size analysis to the Desert Research Institute (DRI) Soils Characterization Laboratory (DRI, Reno, NV, USA) using a Malvern Mastersizer 3000 (Malvern Instruments Inc., Westborough, MA). The particle size range covered was 0.75 to 1500  $\mu\text{m}$  with 34 particle diameter bins reported.

## Results

### Wind conditions

Although saltation threshold was not monitored at the field site, as reported for a nearby sand-dominated surface (Gillies *et al.*, 2015) transport conditions are likely to occur when wind speed

measured at 4 m AGL exceeds  $5 \text{ m s}^{-1}$ . Wind roses for the met towers exterior to the edge of the roughness array for winds  $\geq 6 \text{ m s}^{-1}$  measured at 10 m shows the likely sand transport directions are dominated by winds from the south and south-southeast and the north-northwest (Figure 4). For the case of wind approaching  $\pm 10^\circ$  from perpendicular to the rows, the near surface spatially-averaged wind speed at the normalized distance (ND)  $\approx 137$  (ND = horizontal distance/element height) was reduced by approximately 49% ( $\pm 13\%$ ) compared to the measurement of wind at the same height upwind of the array (Figure 5).

Although a small percentage of wind speeds exceeded  $6 \text{ m s}^{-1}$  at 10 m with approach angles to the array between  $45^\circ$  and  $90^\circ$  from perpendicular to the front of the array during the different collection periods, their effect on the sand collected in the BSNE traps is likely not significant enough to alter the sand flux reduction pattern with increasing distance into the roughness that the array orientation was designed to characterize. The reasons are two-fold: (1) the above threshold winds for this direction range for the east and west sides of the array is between 6% (east) and 12% (west) of the entire time winds were measured to be  $\geq 6 \text{ m s}^{-1}$  at 10 m, and (2) as wind direction approach angle to the front of the array changes between  $45^\circ$  and  $90^\circ$ ,  $\lambda$  changes from 0.052 to 0.033 due to the changing frontal area of the elements, which would reduce the sand flux by 92% (at  $45^\circ$ ) to 81% (at  $90^\circ$ ) according to Gillies *et al.* (2015, Equation (4)) for BSNEs along the centerline of the array.

### Total and vertically distributed mass saltation flux

Four collections of the BSNE traps were made during the duration of the study: October 2, 2015, December 29, 2015, March 17, 2016, and May 16, 2016, with each collection representing multiple transport events. This results in mixing of different transport directions in this bi-modal sand transport wind regime. The further downwind from the leading edge where the saltating particles enter the array, the lesser this mixing effect occurs as it is expected that the flux will diminish with increasing distance into the roughness array as established by Gillies *et al.* (2015). The heights of the sample collection, mass of the trap compartment samples, and the corresponding normalized height (NH) and normalized mass (NM) values are provided in Table II. The height of collection is defined as the height above the surface of the geometric mean position of the rectangular trap opening (Ellis *et al.*, 2009). NH is defined as:  $H_n/H_1$ , where  $H_n$  is the distance above the ground to the position of the geometric mean of a rectangular opening in a trap compartment



**Figure 3.** The modified BSNE style trap (left panel) and the Cox Sand Catcher (right panel) used to collect saltating particles. [Colour figure can be viewed at [wileyonlinelibrary.com](http://wileyonlinelibrary.com)]

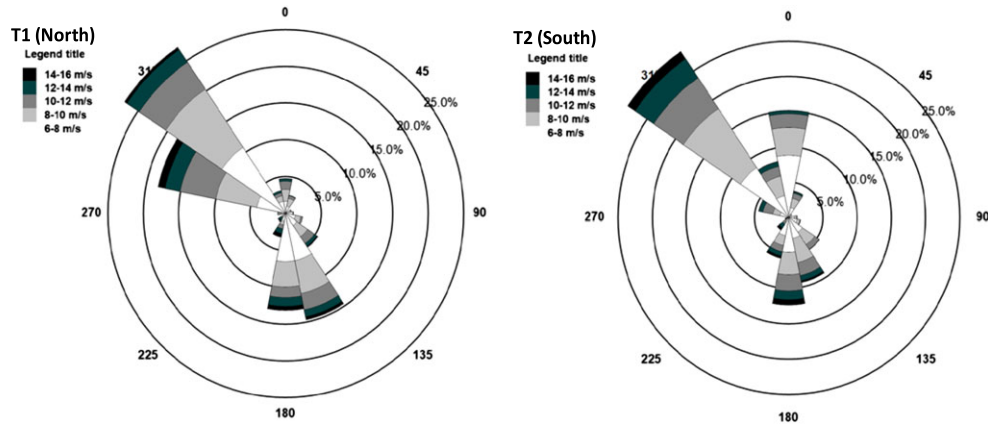


**Figure 4.** Wind roses for the site based on 10 m above ground level (AGL) wind speed and direction measurements at the northern (T1) and southern (T2) edges of the roughness array. [Colour figure can be viewed at [wileyonlinelibrary.com](http://wileyonlinelibrary.com)]

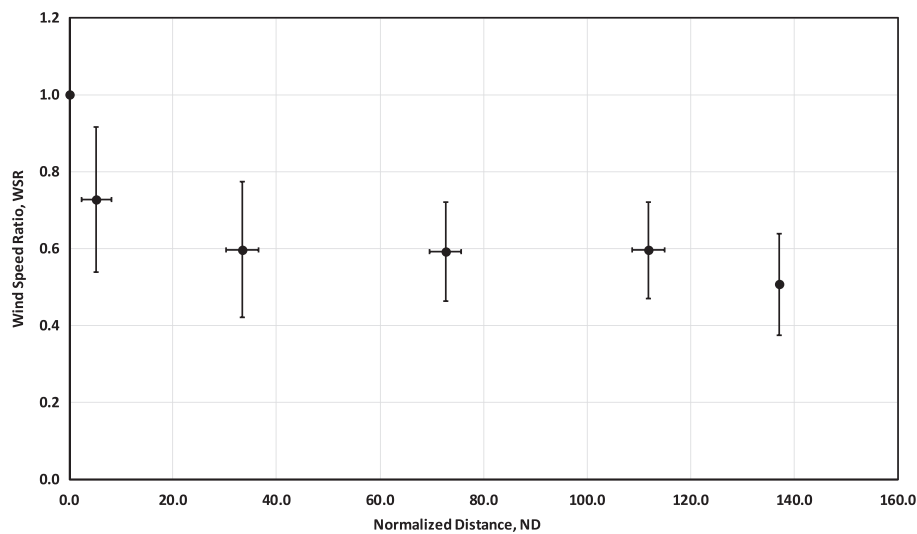


**Figure 5.** The change in near-surface wind speed ratio, WSR, as a function of normalized distance, ND. The x-error bars represent the standard deviation of ND based on the ND for each individual instrument (positions 1–4) in the clusters of instruments from ND = 5.2 ( $\pm 2.9$ ) through to ND = 137 ( $\pm 0$ ) (see Figure 2). The y-error bars represent the standard deviation of the mean WSR based on the five-minute mean WSR values.

and  $H_1$  is the distance above the ground to the position of the geometric mean of the rectangular opening of the lowest trap compartment. NM is defined as:  $\text{mass}_n / \text{mass}_1$ , where  $\text{mass}_n$  is the mass in trap compartment  $n$  divided by the mass in the lowest trap compartment, i.e.  $\text{mass}_1$  at  $H_1$ .

For each collection period the total trap mass (i.e. the sum of the four compartments) divided by the total trap mass exterior to the array defines  $\text{NSF}_T$ , which is plotted as a function of ND for each collection period in Figure 6. These data show a rapid decrease in  $\text{NSF}_T$  with increasing distance into the array from either side. For all sample periods the plots show that sediment transport from south to north was dominant. Although as Figure 6 shows there must have been some transport events from north to south as traps 1 and 2 show higher values than the interior traps.

The strongest signal of change in  $\text{NSF}_T$  as a function of ND is observed in the sequence of traps: 8, 7, 6, 5, 4, which represent the transport condition of sand entering the array on the southern edge and its subsequent movement towards the opposite edge. The relationship between  $\text{NSF}_T$  for the four collection periods and ND, and two trap types, is shown in Figure 7, with the error bars representing the standard deviation of the mean. As observed in previous studies  $\text{NSF}_T$

decreases exponentially with increasing ND up to a point, after which it stabilizes to a constant value (Gillies *et al.*, 2015). For this array of roughness elements  $\text{NSF}_T$  stabilizes at ND  $\approx 160$ –212, with a mean value of 0.10 ( $\pm 0.07$ ). This relationship can be expressed as:

$$\text{NSF}_T = (1 - \text{NSF}_\infty) e^{(-a \text{ND})} + \text{NSF}_\infty \quad (5)$$

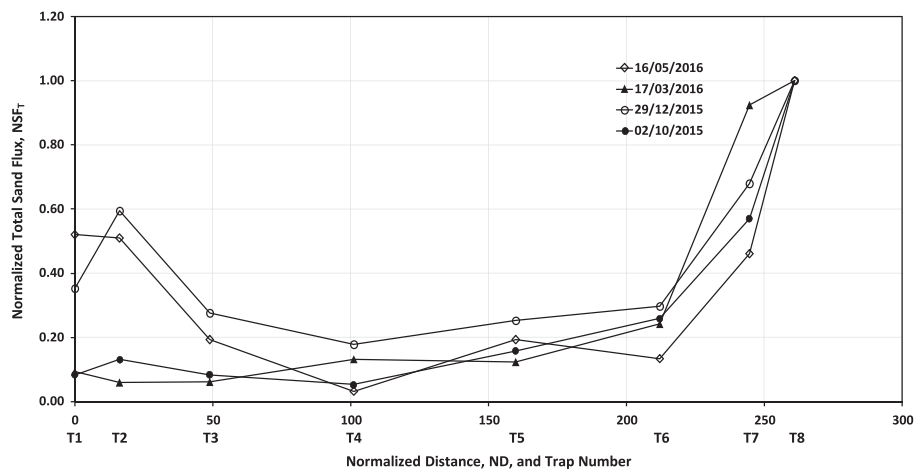
where  $a$  is a dimensional constant and  $\text{NSF}_\infty$  the flux fully adjusted to the step change in roughness.

Equation (5) was not derived formally; rather, it represents a plausible general form to fit the data from a step increase (possibly also step decrease) in roughness. The parameter  $\text{NSF}_\infty$  is straightforward to understand and can be estimated easily either from direct measurement or based on Gillies *et al.*'s (2015) equation (Equation (4)).

NM plotted as a function of NH represents the form of the normalized horizontal flux relationship (NF) based on the vertical variation of mass and defines the rate of change of the particle mass flux above the surface at a measurement position. This relationship for pairs of traps with the same ND from the edges of the roughness array and the mean values

**Table II.** The collected mass and its height of collection for the eight BSNE traps for the four collection periods

	Height (m)	NH	2 October 2015		29 December 2015		17 March 2016		16 May 2016		Mean NM	Standard deviation NM
			Mass (g)	NM	Mass (g)	NM	Mass (g)	NM	Mass (g)	NM		
T1H1 <sup>a</sup>	0.21	1	11.5	1	101.17	1.00	2.79	1	178.78	1.00	1	0.00
T1H2	0.50	2.38	13.43	1.17	30.03	0.30	0.82	0.29	46.47	0.26	0.50	0.44
T1H3	0.83	3.95	NS <sup>b</sup>		15.70	0.16	0.46	0.16	16.93	0.09	0.14	0.04
T1H4	1.28	6.10	NS		7.72	0.08	0.04	0.01	3.93	0.02	0.04	0.03
T2H1	0.18	1	11.07	1	174.89	1.00	1.34	1.00	167.81	1.00	1	0.00
T2H2	0.48	2.62	8.95	0.81	56.17	0.32	0.70	0.52	51.03	0.30	0.49	0.23
T2H3	0.79	4.30	9.42	0.85	22.21	0.13	0.42	0.31	17.73	0.11	0.35	0.35
T2H4	1.26	6.90	9.6	0.87	7.61	0.04	0.13	0.10	4.06	0.02	0.26	0.41
T3H1	0.17	1	8.92	1	73.52	1.00	1.18	1.00	56.98	1.00	1	0.00
T3H2	0.48	2.79	8.34	0.93	25.18	0.34	0.36	0.31	20.28	0.36	0.48	0.30
T3H3	0.78	4.61	7.43	0.83	15.98	0.22	0.68	0.57	9.76	0.17	0.45	0.31
T3H4	1.26	7.39	NS		6.57	0.09	0.49	0.41	3.90	0.07	0.19	0.19
T4H1	0.17	1.00	7.86	1	35.95	1.00	2.05	1.00	5.10	1.00	1	0.00
T4H2	0.47	2.76	7.72	0.98	18.05	0.50	1.52	0.74	5.48	1.07	0.82	0.26
T4H3	0.77	4.55	NS		14.28	0.40	1.36	0.66	1.19	0.23	0.43	0.22
T4H4	1.26	7.41	NS		10.13	0.28	0.78	0.38	3.30	0.65	0.44	0.19
T5H1	0.18	1.00	21.49	1	69.52	1.00	2.35	1.00	67.44	1.00	1	0.00
T5H2	0.48	2.67	9.65	0.45	19.42	0.28	2.03	0.86	14.85	0.22	0.45	0.29
T5H3	0.78	4.34	8.43	0.39	13.44	0.19	0.97	0.41	6.82	0.10	0.27	0.15
T5H4	1.26	7.01	7.41	0.34	8.95	0.13			2.42	0.04	0.17	0.16
T6H1	0.20	1.00	40.02	1	70.30	1.00	3.64	1.00	38.16	1.00	1	0.00
T6H2	0.54	2.70	19.37	0.48	29.98	0.43	3.15	0.87	15.05	0.39	0.54	0.22
T6H3	0.81	4.05	7.57	0.19	21.26	0.30	2.49	0.68	7.44	0.20	0.34	0.23
T6H4	1.29	6.43	9.97	0.25	9.34	0.13	1.34	0.37	2.64	0.07	0.20	0.13
T7H1	0.19	1.00	118.01	1	179.80	1.00	23.01	1.00	150.75	1.00	1	0.00
T7H2	0.49	2.58	31.4	0.27	68.81	0.38	9.13	0.40	42.41	0.28	0.33	0.07
T7H3	0.78	4.16	11.78	0.10	38.57	0.21	5.75	0.25	20.02	0.13	0.17	0.07
T7H4	1.27	6.73	8.76	0.07	11.60	0.06	2.41	0.10	4.27	0.03	0.07	0.03
T8H1	0.20	1.00	230.6	1	331.94	1.00	33.53	1.00	412.79	1.00	1	0.00
T8H2	0.46	2.32	44.86	0.19	72.88	0.22	6.69	0.20	44.07	0.11	0.18	0.05
T8H3	0.80	4.02	14.97	0.06	26.50	0.08	2.02	0.06	12.15	0.03	0.06	0.02
T8H4	1.28	6.44	7.82	0.03	7.76	0.02	1.41	0.04	3.35	0.01	0.03	0.01

<sup>a</sup>T1H1: trap 1, height 1.<sup>b</sup>NS: no sample, trap compartment empty of sand.**Figure 6.** Mean normalized total sand flux,  $NSF_T$  (normalized to trap 8) as a function of normalized distance, ND, for the four collection periods. The lines serve only to emphasize the groupings of the data points by collection period.

of NM representing the four collection periods are shown in Figure 8. The error bars in each case represent the standard deviation of the mean NM. For each trap the vertical flux is well described by an exponential function. The two traps external to the array (i.e. T1 and T8) show a greater rate of

change in NM with NH than do the trap pairs interior to the array (Figure 8).

The  $z_q$  parameter in Equation (1) is the characteristic saltation layer decay height. The change in this variable as a function of ND for the traps combinations: 1, 2, 3, 4, and 8, 7, 6, 5, which

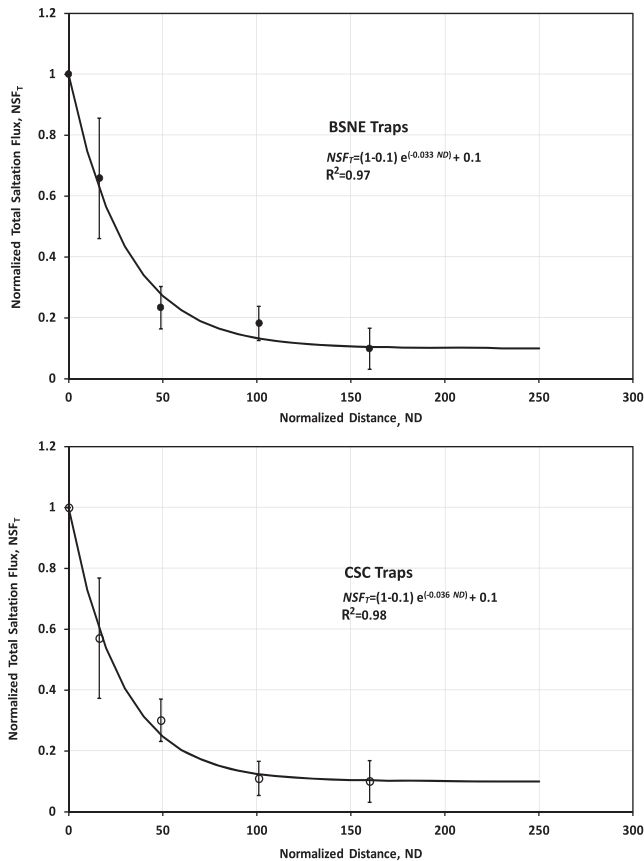


**Figure 7.** Mean normalized total sand flux,  $NSF_T$  as a function of normalized distance,  $ND$ , for trap 4 ( $ND = 160$ ), trap 5 ( $ND = 101.2$ ), trap 6 ( $ND = 48.9$ ), trap 7 ( $ND = 16.3$ ), and trap 8 ( $ND = 0$ ) representing the dominant transport of sand from south to north during the observation period for the BSNE traps (black circles, top panel) and the CSC traps (open circles, bottom panel). Error bars represent the standard deviation of the mean value for the multiple measurement periods.  $NSF_\infty$  was set to the calculated  $NSF_T$  value (0.10) for fitting the relationship defined by Equation (5).

groups them based on having the same  $ND$  values for north to south and south to north transport directions is shown in Figure 9.

### Particle size distribution changes in the vertical saltation flux

The effect of the roughness on the particle size distribution characteristics of the saltation flux in the vertical dimension is revealed through the Malvern Mastersizer-generated data and the calculation of grain size distribution characteristics using the Gradistat particle size analysis software (Blott and Pye, 2001; Kenneth Pye Associates Ltd, UK). Grain size statistics generated by Gradistat are all based on the method of moments and reported as geometric mean diameter (in micrometers). The relationship between mean diameter and  $NH$  for the collection periods: October 2, 2015, December 29, 2015, and March 17, 2016 for the sequence of traps 8, 7, 6, 5 (i.e. south to north transport) is shown in Figure 10. In these cases, the mean diameter decreased with increasing  $NH$  above the surface, and the relationship is well-described, most consistently, by a best-fit logarithmic relationship. Pooling the data by trap number for the three sampling intervals and normalizing the mean diameter by dividing each mean particle diameter by the mean diameter for the highest receptacle (i.e. mean diameter<sub>H4</sub>/mean

diameter<sub>H4</sub>) gave the result that for T8, exterior to the roughness, between the lowest and highest collection heights the mean diameter differed by a factor of 3.0 ( $\pm 1.1$ ). For the three interior traps (7, 6, and 5) the difference in mean diameter from lowest to highest is a consistent decrease by a factor of 2.0 ( $\pm 0.1$ ). The mean diameter at similar collection heights also changes systematically with  $ND$  as shown in Figure 11. The decrease in mean diameter as a function of collection height and  $ND$  is observed for collection heights one ( $\approx 0.2$  m), two ( $\approx 0.5$  m), and three ( $\approx 0.8$  m), and is most consistently described by a logarithmic relationship. For collection height four ( $\approx 1.3$  m), in two of the collection periods an increase in mean diameter was observed moving from outside the array to  $ND = 48.9$ , thereafter little variation of mean diameter between  $ND = 48.9$  and  $ND = 159.9$  was observed at this height.

By partitioning the mass flux in each trap compartment by the mass fraction associated with the eight particle size bins for the sand-sized components of the material in each trap compartment (i.e. 750  $\mu\text{m}$ , 375  $\mu\text{m}$ , 225  $\mu\text{m}$ , 175  $\mu\text{m}$ , 137.5  $\mu\text{m}$ , 112.5  $\mu\text{m}$ , 87.5  $\mu\text{m}$ , and 68.7  $\mu\text{m}$ ),  $z_q$  for each of these particle diameters can be estimated at the four measurement positions:  $ND = 0$ , 16.3, 48.9, and 101.2. The regression-derived value for  $z_q$  as a function of mean diameter for the available data (from both transport directions), is shown in Figure 12. As this Figure 12 shows,  $z_q$  increases for each particle diameter with increasing distance into the array, and as particle diameter decreases,  $z_q$  increases at a faster rate. The rate of change of  $z_q$  with increasing  $ND$  (i.e.  $m$  term in  $z_q = m(ND) + b$ , for each particle diameter in Figure 11), as a function of particle diameter is shown in Figure 13 and is well-defined by a power relationship.

## Discussion

### Effect of roughness on the mass flux

As previously observed by Gillies *et al.* (2006, 2015),  $NSF_T$  scales as a function of  $\lambda$ . Gillies *et al.*'s (2015) equation (Equation (4)) predicts that for  $\lambda = 0.045$ , the equilibrium  $NSF_T$  for an array of large roughness elements should be 0.10. The mean  $NSF_T$  for the interior of the array for this experiment for  $ND = 159.9$  was 0.10 ( $\pm 0.07$ ), which matches the model prediction very closely. The roughness adjusted  $NSF_T$  value was based on using measurements at multiple heights above the surface and as can be seen from Figure 7, matches closely the saltation flux reduction pattern measured at the same height low to the ground and over a wider area.

The rate of change of  $NSF_T$  with increasing  $ND$  for that portion of the curve shown in Figure 7 before the fully-adjusted flux is attained (i.e.  $ND = 0$  to  $ND = 101$ ) for this roughness array can be compared with other experiments that have measured the effect of roughness on  $NSF_T$ . Defining this portion of the curve similarly to Gillies *et al.* (2006, 2015) and Gillies and Lancaster, 2013) as  $NSF_T = a e^{(-B ND)}$ , the value of  $B$  for this experiment for the BSNE trap data is  $-0.17$  and  $-0.021$  for the CSC trap data. Given the stochastic and variable nature of aeolian transport (e.g. Gares *et al.*, 1996; Stout and Zobeck, 1997; Jackson *et al.*, 2006) and the variability in wind direction, transport and surface conditions among the available studies, the values of  $B$  for this experiment fit closely with the predicted value of  $B = -0.016$  based on the relationship presented by Gillies *et al.* (2015, their figure 11) that uses data from three experiments. In general, the new Owens Lake  $NSF_T$  relationships fit quite well with previous measurements, which indicates that the established scaling relationship between sand flux and  $\lambda$  (Gillies *et al.*, 2015; Equation (4)) is very robust at least for

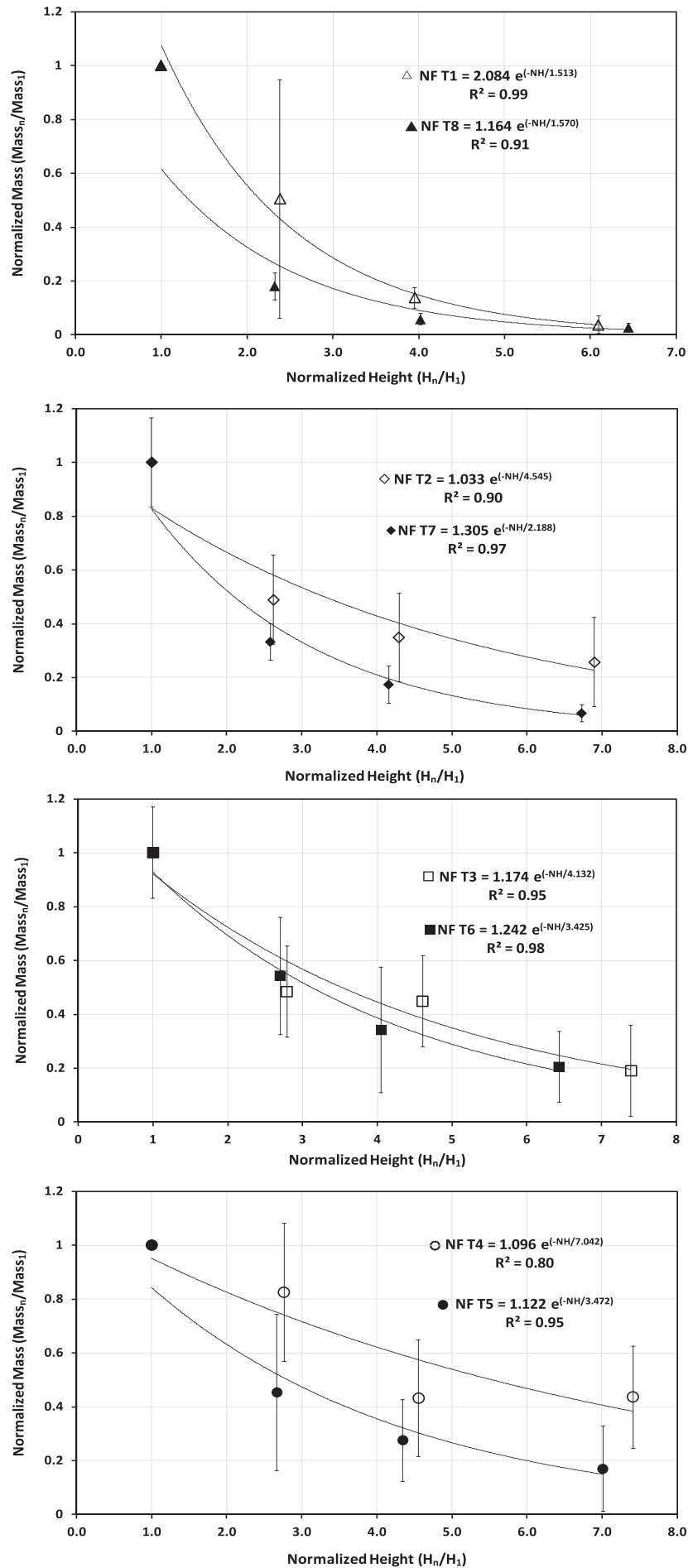


**Figure 8.** The relationship between normalized mass, NM, and normalized height, NH, as a function of shared trap positions at ND = 0 (traps 1 and 8, top panel), ND = 16.3 (traps 2 and 7, top middle panel), ND = 48.9 (traps 3 and 6, bottom middle panel), and ND = 101.2 (traps 4 and 5, bottom panel).



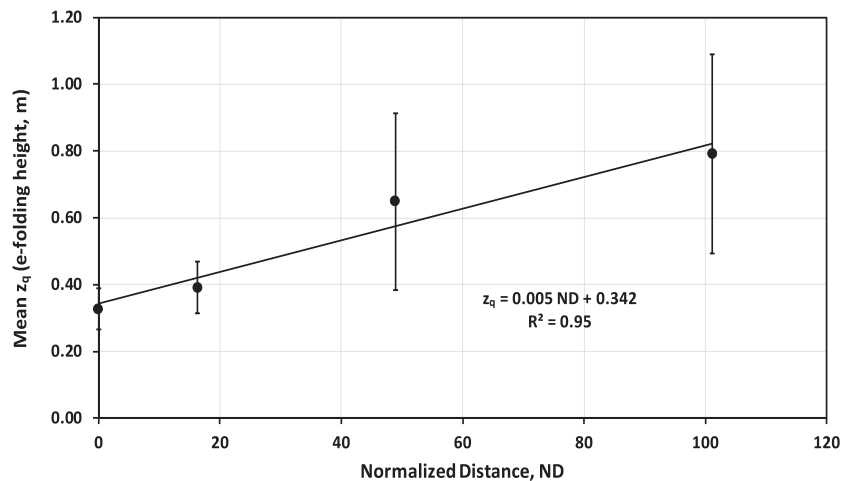


**Figure 9.** The mean e-folding height (i.e.  $z_q$  in Equation (1)) for the sequence of four traps for sand transport direction from north to the south and south to north at equivalent normalized distance, ND, positions. Error bars represent the standard deviation of the mean.

roughness that is relatively closely spaced and of all the same height. Chappell and Webb (2016) argue that  $\lambda$  is less successful in predicting shear stress partitioning and shelter effects for superposed roughness that covers a range of element heights and widths, which may also reduce the applicability of the Gillies *et al.* (2015) equation for estimating the effect of non-homogeneous roughness on sand transport. Their equation does, however, appear very useful for designing arrays of large roughness elements to control saltation flux and the associated dust emissions.

### Effect of roughness on the particle size distribution of the saltators

In general, for all trap samples the mean particle diameter decreases as a function of height above the surface (for  $H > 0.17$  m), exterior and interior to the roughness. This matches the observations of Li *et al.* (2008) for wind tunnel tests using sand of mixed size and this pattern of decreasing grain diameter with height has also been observed by others in wind tunnel experiments (e.g. Williams, 1964) and in field measurements (Gillies *et al.*, 2013), but as noted earlier this pattern is not universal (e.g. Williams, 1964; Xing, 2007; Speirs *et al.*, 2008; Gillies *et al.*, 2013). The reduction of mean particle diameter with passage of the saltators through the roughness array suggests that there is preferential removal of coarser grains through the height of the saltation layer. The removal is likely due to the preferential trapping of grains in zones of wind shear in the lee of the roughness elements that are below the threshold to keep particles in motion as well as long enough for particle inertia to be insufficient to carry them through to a zone of above threshold conditions. Deposits of sand were observed in the lee of roughness elements, most notably for the rows nearest the edges (i.e. rows 1 to 8 and 32 to 40).

### Effect of roughness on the mass flux in the vertical dimension

This new data set, for the first time, allowed for an examination of the effect of roughness on the mass flux based on integration in the vertical dimension using the multi-height BSNE traps. As Figures 9–11 show, the saltation flux is altered by its interaction with the roughness array in the horizontal and vertical

dimensions. With increasing distance into the array the sand in saltation shows an increase in  $z_q$  (Figure 9), which can, in part, be explained by the diminishing total mass flux. In addition, the mean particle diameter at all but the top measurement position decreases with increasing distance into the array (Figure 11). The particle size distribution data offers some explanatory power for why these patterns occur.

According to Martin and Kok (2017a), for saltating sand over an essentially roughness-element-free and relatively flat surface with no sediment supply restrictions, mean particle speed and  $z_q$  remain constant with changing surface shear stress ( $\tau$ , in  $\text{N m}^{-2}$ ) above threshold. Martin and Kok (2017a) note that  $z_q$  is not constant for all surfaces, but is likely controlled by the particle size distribution of the source sand. In the case studied in our experiment, where the saltating sand encounters and interacts with the large-scale roughness, there are profound changes in the mass flux as well as  $z_q$  as a function of particle diameter. As  $z_q$  increases with distance into the array it suggests that particle speeds are changing as the saltating particles move through the array at least to  $\text{ND} = 101.2$ . An increase in  $z_q$  represents an increase in the characteristic saltator hop height (Owen, 1964; Ungar and Haff, 1987; Namikas, 2003; Kok, 2010). Since hop height is determined by the speed at which particles are launched from the surface (Equation (3)), which in turn depends on the mean particle speed (Owen, 1964; Ungar and Haff, 1987; Kok, 2010), our observation of increasing  $z_q$  into the roughness array implies that the mean particle speed also increases for all particle sizes and with increasing distance into the roughness.

The observed effect of  $z_q$  increasing with increasing distance into the array and with decreasing particle diameter in the presence of the roughness is different from that observed for saltation in the absence of superposed roughness. Martin and Kok (2017b) report for unconstrained saltation on sand sheets,  $z_q$  increases with particle diameter up to the modal diameter of the sand (that is of the source sand) and then decreases for particle diameters less than the modal diameter.

We suggest that the effects on  $z_q$  and mean diameter in the case of the superposed roughness are occurring due to the reduction in saltation flux caused by the presence of the roughness elements. Mechanisms that are driving the loss are the change in wind shear exerted on the saltation layer with increasing distance into the array due to shear stress partitioning as the wind adjusts to this step change in roughness (Raupach *et al.*, 1993; Gillies *et al.*, 2007), and the interaction of the saltation with the roughness elements (Gillies and Lancaster, 2013).

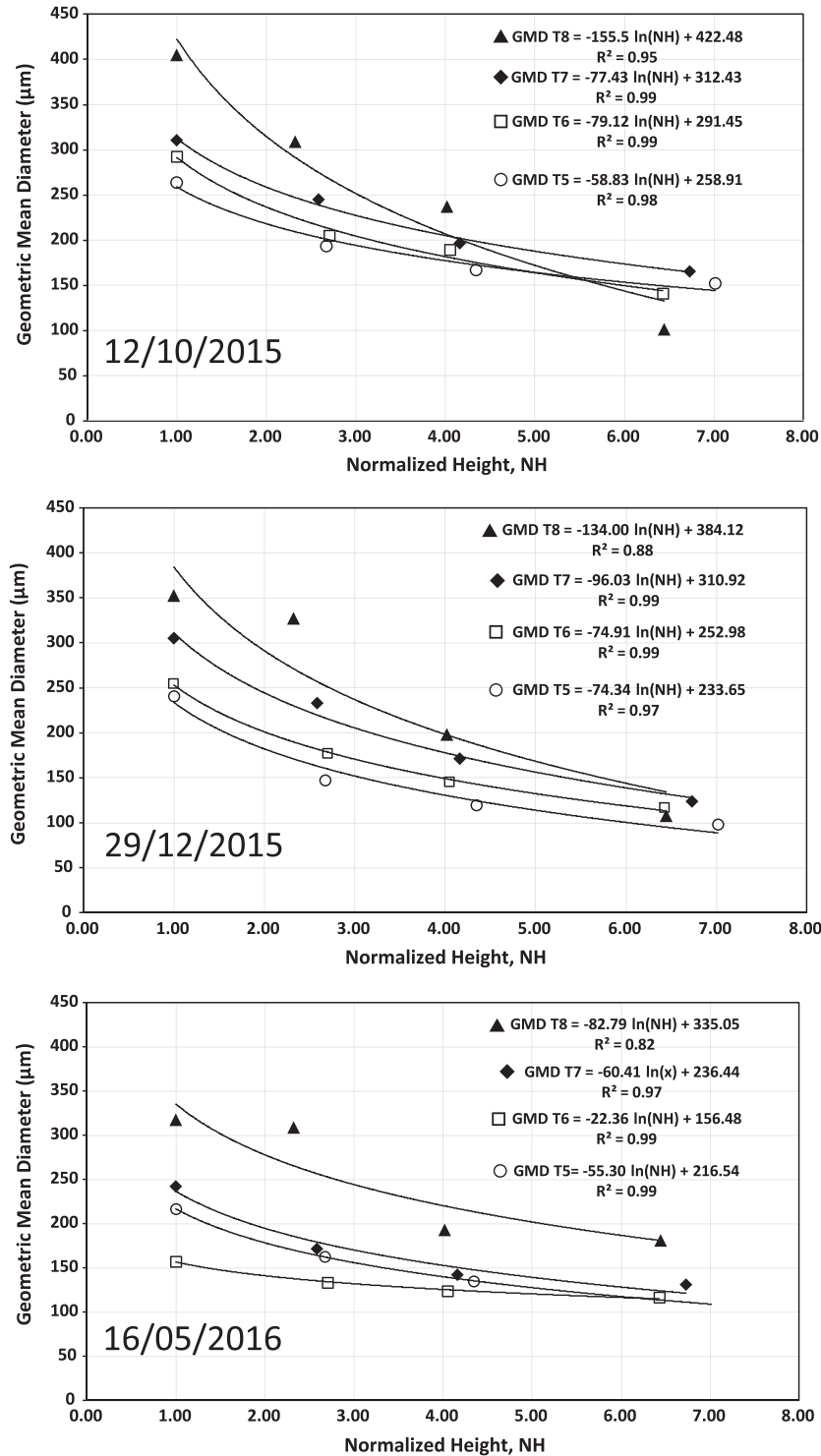


**Figure 10.** The relationship between mean particle diameter and normalized height, NH, for three collection periods for the trap grouping 8, 7, 6, 5, representing the south to north sand transport direction.

According to Gillies *et al.* (2007), the shear stress ratio ( $R$ , Raupach *et al.*, 1993) for  $\lambda = 0.045$  at  $\text{ND} > 127.5$ , should be  $\approx 0.62$ , which would reduce the shear stress on the surface ( $\tau_s$ , in  $\text{N m}^{-2}$ ) at that position by  $\approx 38\%$ . Applying the Shao (2005) scaling relationship between shear stress, expressed as the shear velocity  $u_*$  (in  $\text{m s}^{-1}$ , where  $\tau = \rho_a u_*^2$  [ $\rho_a$  is air density, in  $\text{kg m}^{-3}$ ]) and sand flux ( $q$ , in  $\text{kg m}^{-1} \text{s}^{-1}$ ):

$$q = C_{\text{Shao}} \frac{\rho_a u_*^3}{g} \left( 1 - \left( \frac{u_{*t}}{u_*} \right)^2 \right) \quad (6)$$

where  $C_{\text{Shao}}$  is a coefficient and  $u_{*t}$  is the threshold shear velocity, the reduction in  $q$  at  $\text{ND} = 127.5$  should be  $\approx 76\%$

compared to the flux external to the array. At  $\text{ND} < 127.5$  the partitioning of shear stress between the roughness elements and the surface will be changing as a function of ND into the array at an approximately exponential rate to approximately  $\text{ND} = 73$  to  $93$  (Gillies *et al.*, 2007). Gillies and Lancaster (2013) observed first that the reduction in saltation flux observed in an array of large roughness elements was greater than could be attributed to shear stress partitioning by itself and suggested the physical interaction of the saltating sand with the roughness and the environment around the elements accounted for the additional reduction in sand flux by the elements physically impeding the movement of the particles. The

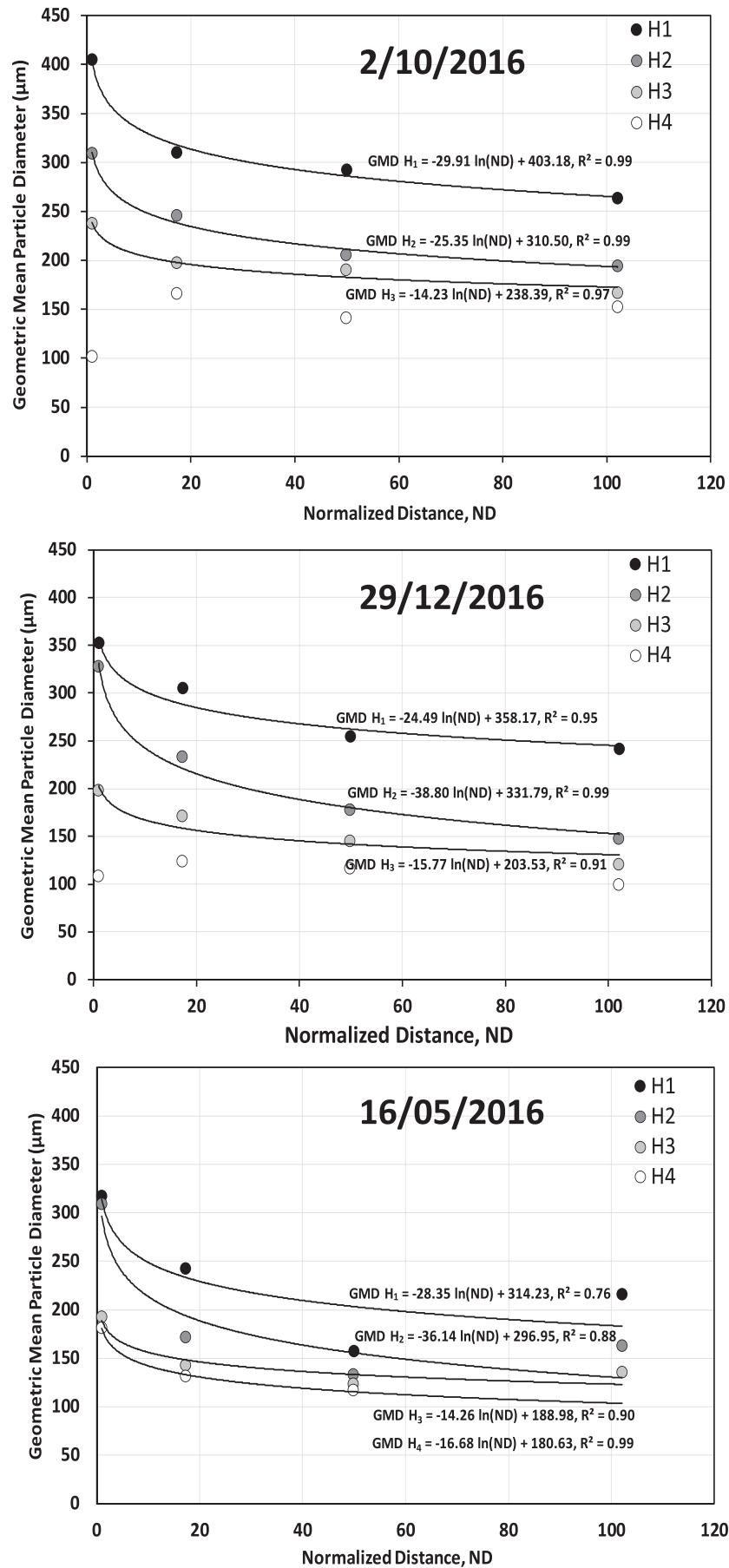


**Figure 11.** Observed change in the mean particle diameter as a function of normalized distance, ND, for trap grouping 8, 7, 6, 5, characterizing the south to north transport direction for three monitoring periods.

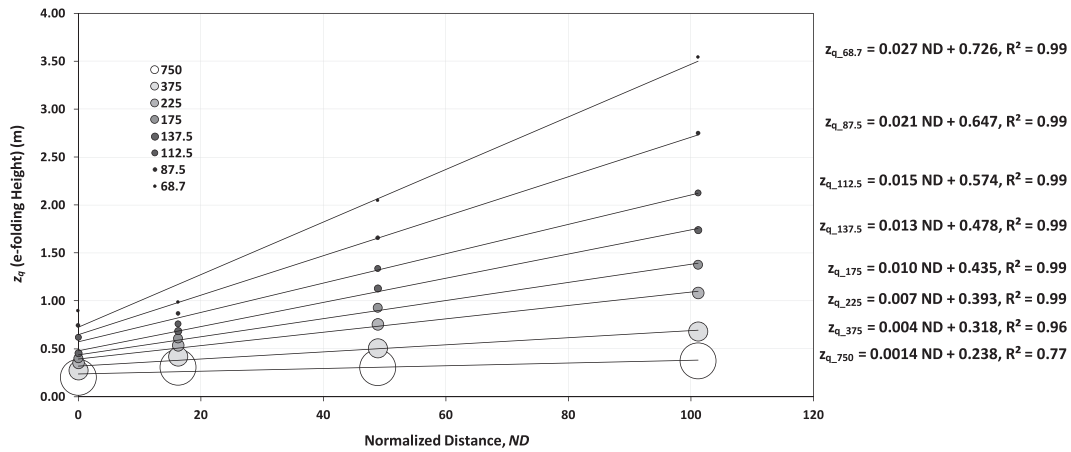


**Figure 12.** The e-folding height,  $z_q$ , as a function of normalized distance,  $ND$ , and particle diameter.

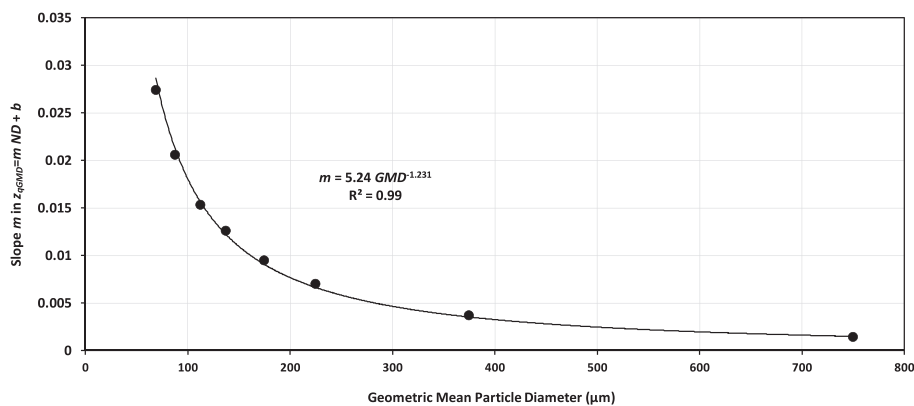


**Figure 13.** The rate of change in  $z_q$  as a function of particle diameter as defined by the  $m$  term in the relationship  $z_q = m ND + b$  for each particle size bin.

shear stress partitioning, the physical dimensions of the roughness, and their distribution on the surface result in a reduction in mass flux through the roughness as defined by Figure 7.

The loss of particles from the saltating population explains why the particles appear to increase their mean speed as indicated by the increase in  $z_q$  (Figures 12 and 13). A plausible mechanism for this is that slower particles are being preferentially removed as they have a reduced probability of making it deeper into the roughness. Slower moving particles are less likely to have the momentum necessary to carry them through zones of lower shear stress created by the presence of the roughness. Hence as saltators of a given size range pass through the array, their mean speed increases as the distribution of speed is increasingly truncated at the lower end of the distribution, which is supported by the observed increase in  $z_q$  with increasing distance into the array (Figure 9). The wind close to the surface decreases with increasing distance into the array (Figure 5), so the particles cannot be gaining speed through interaction with higher speed winds.

The measurements of particle size resolved flux exterior to the roughness provide additional information on the scaling of sand flux with wind speed under these supply-limited conditions. Martin and Kok (2017a) demonstrated with saltation flux data that the saltation layer height does not change with  $u_*$ , implying that mean particle speed also remains constant with  $u_*$ . When the flux versus height relationships are binned by particle diameter, it is observed (Figure 12 at  $ND = 0$ ) that  $z_q$  increases with decreasing particle diameter, implying

that for this sand transport condition the smaller diameter particles are travelling at a faster speed than the larger diameter particles, suggesting in this case that particle launch velocity increased with decreasing particle diameter. A likely reason why  $z_q$  increases with particle diameter exterior to the array, as opposed to the observation of Martin and Kok (2017b) showing an increase in  $z_q$  up to the modal diameter, followed thereafter by a decrease, is due to the supply-limited sediment conditions on the playa. Under supply-limited conditions, particle speed is controlled by the restitution coefficient, determined by the soil surface condition, and the wind speed. Smaller diameter particles enter into the array with greater speed than larger ones so only the fastest particles in each particle size bin make it deep into the roughness array, and hence  $z_q$  increases for decreasing particle diameter.

## Conclusions

The effect of a step change in macro-roughness on the saltation process was examined at the full scale in the atmospheric boundary layer. The saltation flux was profoundly altered in the horizontal and vertical dimensions as a result of its interactions with the roughness. The horizontal flux was reduced by 90% ( $\pm 7\%$ ) at a distance of  $\approx 150$  roughness element heights into the array as predicted by the empirical model of Gillies *et al.* (2015), for an array of roughness with  $\lambda = 0.045$ . These



results provide further corroboration of the robust nature of this simple model to estimate sand flux reduction for roughness elements of height dimension of  $\approx 0.4\text{ m}$  that are evenly distributed across space, providing increased confidence that it can be effectively used to engineer roughness arrays to meet sand flux reduction targets.

Measurements of the saltation flux characteristics in the vertical dimension, including particle size characteristics, revealed that with increasing distance into the array mean particle diameter became smaller, reducing in size as a function of distance as well as a logarithmic function of height above the surface. The distribution of the saltation mass flux in the vertical as a function of increasing distance into the roughness array, trended towards a more uniform distribution, although it remained exponential in form. This is only possible if there is a diminishment of the particle flux, which was observed. This diminishment of flux appears to be associated with the loss of the slower speed particles so that with increasing distance into the roughness, the mean particle speed for a given particle diameter is shifted to a higher value, but remains less than the maximum speed of the initial distribution of speeds. It will require additional experimentation to resolve the behavior of the particle speed distribution as a function of particle diameter through measurement of actual particle speeds within superposed roughness for both supply and transport limited conditions. Further information on the particle speed distribution in the presence of the roughness would also be informative on how the roughness modulated saltation flux affects the dust emission process.

**Acknowledgements**—The authors are grateful for the financial, logistical, technical, and intellectual support received from the Great Basin Unified Air Pollution Control District, Bishop, CA, and the City of Los Angeles Department of Water and Power, Keeler, CA, during the execution of this project. US National Science Foundation (NSF) grant AGS-1358621 to J.F.K. also supported this research. The authors would also like to acknowledge the Desert Research Institute personnel who worked on the project, especially during the installation and removal of the roughness elements and all the attendant instrumentation: Yannick Agnan, Dave Campbell, Eden Furtak-Cole, Jesse Juchter, Mark McDaniel, and Davis Zhu.

## References

- Al-Awadhi JM. 2014. The effect of a single shrub on wind speed and nabkhas dune development: a case study in Kuwait. *International Journal of Geosciences* **5**: 20–26. <https://doi.org/10.4236/ijg.2014.51004>.
- Anderson RS. 1987. A theoretical model for aeolian impact ripples. *Sedimentology* **34**: 943–956.
- Andreotti B. 2004. A two-species model of aeolian sand transport. *Journal of Fluid Mechanics* **510**: 47–70. <https://doi.org/10.1017/S0022112004009073>.
- Bagnold RA. 1941. *The Physics of Blown Sand and Desert Dunes*. Chapman and Hall: London; 265.
- Blott SJ, Pye K. 2001. GRADISTAT: a grain size distribution and statistics package for the analysis of unconsolidated sediments. *Earth Surface Processes and Landforms* **26**(11): 1237–1248.
- Chappell A, Webb NP. 2016. Using albedo to reform wind erosion modelling, mapping and monitoring. *Aeolian Research* **23**(Part A): 63–78. <https://doi.org/10.1016/j.aeolia.2016.09.006>.
- Chepil RS. 1945. Dynamics of wind erosion: I. Nature of movement of soil by wind. *Soil Science* **60**: 305–320.
- Claudin P, Andreotti B. 2006. A scaling law for aeolian dunes on Mars, on Earth and subaqueous ripples. *Earth and Planetary Science Letters* **252**: 30–44. <https://doi.org/10.1016/j.epsl.2006.09.004>.
- Durán O, Claudin P, Andreotti B. 2011. On aeolian transport: grain scale interactions, dynamical mechanisms and scaling laws. *Aeolian Research* **3**: 243–270. <https://doi.org/10.1016/j.aeolia.2011.07.006>.
- Ellis JT, Li B, Farrell EJ, Sherman DJ. 2009. Protocols for characterizing aeolian mass-flux profiles. *Aeolian Research* **1**(1–2): 19–26. <https://doi.org/10.1016/j.aeolia.2009.02.001>.
- Farrell EJ, Sherman DJ. 2006. Process-scaling issues for aeolian transport modelling in field and wind tunnel experiments: roughness length and mass flux distributions. *Journal of Coastal Research* **39**(special issue): 384–389.
- Farrell EJ, Sherman DJ. 2013. Estimates of the Schmidt number for vertical flux distributions of wind-blown sand. *Proceedings, 12th International Coastal Symposium, Journal of Coastal Research, Plymouth, UK*. DOI: <https://doi.org/10.2112/SI65-218.1>
- Farrell EJ, Sherman DJ, Ellis JT, Li B. 2012. Vertical distribution of grain size for wind blown sand. *Aeolian Research* **7**: 51–61. <https://doi.org/10.1016/j.aeolia.2012.03.003>.
- Fryrear DW. 1986. A field dust sampler. *Journal of Soil and Water Conservation* **41**: 117–120.
- Gares PA, Davidson-Arnott RGD, Bauer BO, Sherman DJ, Carter RWG, Jackson DWT, Nordstrom KF. 1996. Alongshore variations in aeolian sediment transport, Carrick Finn Strand, Ireland. *Journal of Coastal Research* **12**: 673–682.
- Gillies JA, Lancaster N. 2013. Large roughness element effects on sand transport, Oceano Dunes, California. *Earth Surface Processes and Landforms* **38**(8): 785–792. <https://doi.org/10.1002/esp.3317>.
- Gillies JA, Nickling WG, King J. 2006. Aeolian sediment transport through large patches of roughness in the atmospheric inertial sublayer. *Journal of Geophysical Research – Earth Surface* **111** F02006. DOI: <https://doi.org/10.1029/2005JF000434>.
- Gillies JA, Nickling WG, King J. 2007. Shear stress partitioning in large patches of roughness in the atmospheric inertial sublayer. *Boundary-Layer Meteorology* **122**(2): 367–396. <https://doi.org/10.1007/s10546-006-9101-5>.
- Gillies JA, Nickling WG, Tilson M. 2013. Frequency, magnitude, and characteristics of aeolian sediment transport: McMurdo Dry Valleys, Antarctica. *Journal of Geophysical Research: Earth Surface* **118**: 1–19. <https://doi.org/10.1029/2012JF002473>.
- Gillies JA, Nield JM, Nickling WG. 2014. Wind speed and sediment transport recovery in the lee of a vegetated and denuded nebkha within a nebkha dune field. *Aeolian Research* **12**: 135–141. <https://doi.org/10.1016/j.aeolia.2013.12.005>.
- Gillies JA, Nickling WG, King J, Lancaster N. 2010. Modeling aeolian sediment transport thresholds on physically rough Martian surfaces: a shear stress partitioning approach. *Geomorphology* **121**: 15–21. <https://doi.org/10.1016/j.geomorph.2009.1002.1016>.
- Gillies JA, Nickling WG, Tilson M, Furtak-Cole E. 2012. Wind-formed gravel bed forms, Wright Valley, Antarctica. *Journal of Geophysical Research: Earth Surface* **117** F04017. DOI: <https://doi.org/10.1029/2012JF002378>.
- Gillies JA, Green H, McCarley-Holder G, Grimm S, Howard C, Barbieri N, Ono D, Schade T. 2015. Using solid element roughness to control sand movement: Keeler Dunes, Keeler, California. *Aeolian Research* **18**: 35–46. <https://doi.org/10.1016/j.aeolia.2015.05.004>.
- Jackson NL, Sherman DJ, Hesp PA, Klein AHF, Ballasteros F, Nordstrom KF. 2006. Small-scale spatial variations in aeolian sediment transport on a fine-sand beach. *Journal of Coastal Research* **39**(special issue): 379–383.
- Kok JF. 2010. An improved parameterization of wind-blown sand flux on Mars that includes the effect of hysteresis. *Geophysical Research Letters* **37**(12) L12202. DOI: <https://doi.org/10.1029/2010gl043646>.
- Kok JF, Parteli EJR, Michaels TI, Bou Karam D. 2012. The physics of wind-blown sand and dust. *Reports on Progress in Physics* **75**: 106901. <https://doi.org/10.1088/0034-4885/75/10/106901>.
- Lancaster N, Nickling WG, Gillies JA. 2010. Sand transport by wind on complex surfaces: field studies in the McMurdo Dry Valleys, Antarctica. *Journal of Geophysical Research – Earth Surface* **115** F03027. DOI: <https://doi.org/10.1029/2009JF001408>.
- Li ZS, Feng DJ, Wu SL, Borthwick AGL, Ni JR. 2008. Grain size and transport characteristics of non-uniform sand in aeolian saltation. *Geomorphology* **100**: 484–493. <https://doi.org/10.1016/j.geomorph.2008.01.016>.
- Martin RL, Kok JF. 2017a. Linear scaling of wind-driven sand flux with shear stress. *Science Advances* **3**: e1602569. <https://doi.org/10.1126/sciadv.1602569>.
- Martin RL, Kok JF. 2017b. Equal susceptibility and size-selective mobility in aeolian saltation. *arXiv*: 1707.09964.

- Namikas SL. 2003. Field measurement and numerical modeling of aeolian mass flux distributions on a sandy beach. *Sedimentology* **50**(2): 303–326. <https://doi.org/10.1046/j.1365-3091.2003.00556.x>.
- Ono D, Kiddoo P, Howard C, Davis G, Richmond K. 2011. Application of a combined measurement and modeling method to quantify windblown dust emissions from the exposed playa at Mono Lake, California. *Journal of the Air and Waste Management Association* **61**: 1036–1054.
- Owen PR. 1964. Saltation of uniform grains in air. *Journal of Fluid Mechanics* **20**: 225–242.
- Parteli ER, Durán O, Bourke MC, Tsoar H, Pöschel T, Herrmann H. 2014. Origins of barchan dune asymmetry: insights from numerical simulations. *Aeolian Research* **12**: 121–133. <https://doi.org/10.1016/j.aeolia.2013.12.002>.
- Raupach MR, Gillette DA, Leys JF. 1993. The effect of roughness elements on wind erosion threshold. *Journal of Geophysical Research* **98**(D2): 3023–3029.
- Schmerler E, Katra I, Kok JF, Tsoar H, Yizhaq H. 2016. Experimental and numerical study of Sharp's shadow zone hypothesis on sand ripple wavelength. *Aeolian Research* **22**: 37–46. <https://doi.org/10.1016/j.aeolia.2016.05.006>.
- Shao Y. 2001. A model for mineral dust emission. *Journal of Geophysical Research* **106**(D17): 20239–20254. <https://doi.org/10.1029/2001JD900171>.
- Shao Y. 2005. A similarity theory for saltation and application to aeolian mass flux. *Boundary-Layer Meteorology* **115**: 319–338.
- Shao Y, Raupach MR, Findlater PA. 1993. The effect of saltation bombardment on the entrainment of dust by wind. *Journal of Geophysical Research* **98D**: 12719–12726.
- Sherman DJ, Farrell EJ. 2008. Aerodynamic roughness lengths over movable beds: comparison of wind tunnel and field data. *Journal of Geophysical Research – Earth Surface* **113**: F02S08. <https://doi.org/10.1029/2007JF000784>
- Sørensen M. 1985. Estimation of some aeolian saltation transport parameters from transport rate profiles. *Proceedings of International Workshop on the Physics of Blown Sand*, University of Aarhus, Aarhus.
- Speirs JC, McGowan HA, Neil DT. 2008. Polar eolian sand transport: grain characteristics determined by an automated electron microscope (QEMSCAN). *Arctic, Antarctic and Alpine Research* **40**(4): 731–743. [https://doi.org/10.1657/1523-0430\(07-029\)\[5BSPEIRS\]5D2.0.CO;2](https://doi.org/10.1657/1523-0430(07-029)[5BSPEIRS]5D2.0.CO;2).
- Stout JE, Zobeck TM. 1997. Intermittent saltation. *Sedimentology* **44**(5): 959–970.
- Ungar JE, Haff PK. 1987. Steady state saltation in air. *Sedimentology* **34**: 289–299.
- White BR, Mounla H. 1991. An experimental study of Froude number effect on wind-tunnel saltation. *Acta Mechanica Supplement* **1**: 145–157.
- Williams G. 1964. Some aspects of the aeolian saltation load. *Sedimentology* **29**: 409–417.
- Wolfe SA, Nickling WG. 1994. The morphology and origin of nabkhas, region of Mopti, Mali, West Africa. *Journal of Arid Environments* **28**: 13–30.
- Xing M. 2007. The harmonious character in equilibrium aeolian transport on mixed sand bed. *Geomorphology* **86**: 230–242. <https://doi.org/10.1016/j.geomorph.2006.08.015>.
- Zhang Z, Dong Z, Qian G. 2017. Field observations of the vertical distribution of sand transport characteristics over fine, medium and coarse sand surfaces. *Earth Surface Processes and Landforms* **42**(6): 889–902. <https://doi.org/10.1002/esp.4045>.